Turkish Journal of Physics
http://journals.tubitak.gov.tr/physics/
Research Article
Turk J Phys
(2014) 38: 238 – 244
© TÜBİTAK
doi:10.3906/fiz-1310-3

Annealing effects of ZnO thin films on p-Si(100) substrate deposited by PFCVAD

Kamuran KARA[1,*], **Ebru ŞENADIM TÜZEMEN**[2], **Ramazan ESEN**[3]
[1]Department of Physics, Faculty of Science, İstanbul University, İstanbul, Turkey
[2]Department of Physics, Faculty of Science, Cumhuriyet University, Sivas, Turkey
[3]Department of Physics, Faculty of Science, Çukurova University, Adana, Turkey

Received: 07.10.2013 • **Accepted:** 06.05.2014 • **Published Online:** 11.06.2014 • **Printed:** 10.07.2014

Abstract: In this study, ZnO films were prepared on p-Si substrates using the pulsed filtered cathodic vacuum arc deposition (PFCVAD) method. We report the effect of annealing temperature on structural and optical properties. The crystallographic structure and the size of the crystallites in the films were studied by means of X-ray diffraction. The films had a weak peak (100) orientation at $2\theta = \sim 32°$. X-ray diffraction analysis of the as-deposited ZnO and the film annealed at 850 °C showed a strong ZnO (002) diffraction peak centered at 34.1° and 34.5°, respectively. The (004) peak was seen for film annealed at 850 °C. ZnO film annealed at 850 °C had higher grain size and better crystallinity. Optical properties of the ZnO films were studied using a UV-Vis-NIR spectrophotometer. The optical band gap of the films was determined using the reflectance spectra by means of the Kubelka–Munk formula. From the optical properties, the band gap energy estimated for films as-deposited and annealed at 850 °C was 3.00 and 3.28 eV, respectively. The Raman scattering spectra of the films was observed at a laser power of 2 mW.

Key words: ZnO, Kubelka–Munk function, Raman scattering

1. Introduction

With a large exciton binding energy (around 60 meV at room temperature) and a wide and direct band gap [1], ZnO thin films have attracted great attention. Good transmission properties in the visible range and an exciton binding energy of up to 60 meV make it one of the more promising candidates for fabricating surface acoustic wave instruments, gas sensors, solar cells, and heat-reflecting windows [2–4].

ZnO/Si heterojunctions have attracted more and more attention. In particular, from the point of view of the combination with advanced Si-microelectronics technology, ZnO growth on Si is very valuable [5]. Silicon is one of most abundant and most important semiconductor materials, and it has been used in a broad range of applications such as photoelectrochemical cells, solar cells, field emission devices, and photodetectors [6–10]. Due to the abovementioned properties, some groups have conducted studies on the production of ZnO thin film on Si in recent years [4,11]. Different techniques for the preparation of ZnO films on Si have been used, including plasma-enhanced metalorganic chemical vapor deposition [12], RF active sputtering technique [13], sol-gel dip coating [14], pulsed laser deposition [15], plasma-assisted metalorganic chemical vapor deposition [16], chemical vapor deposition method [17], atomic layer deposition [18], ultra-high vacuum radio frequency magnetron sputtering method [19], and reactive direct current sputtering [20].

*Correspondence: kamurankara@mynet.com

In this paper, we performed the deposition of ZnO thin films on silicon by pulsed filtered cathodic vacuum arc deposition (PFCVAD) technique at room temperature and studied their structural and optical properties.

2. Experimental

ZnO thin films were grown on Si(100) substrate by PFCVAD. The details of the deposition system were published in an earlier study [21]. In this work, the substrate temperature was kept at room temperature during growth. The base pressure of the deposition chamber was $\sim 10^{-5}$ Torr and the working pressure was $\sim 3.33 \times 10^{-2}$ Torr. The base pressure and working pressure were controlled by SRS Stanford Research Systems Model PPM 100. High purity (99.999% pure) oxygen was introduced into the chamber and controlled by a multigas controller. ZnO thin films were grown using a metallic target (Zn, 99.99%, 1 mm in diameter). After deposition, a film was oxidized at 850 °C for 1 h in air.

In order to investigate the crystalline properties, films grown on Si(100) substrate were examined by θ-2θ X-ray diffraction (XRD) measurements. For XRD studies, we used a Rigaku Miniflex system with CuKα radiation (λ = 1.54059 Å). Raman measurements were carried out with a Bruker SENTERRA Dispersive Raman Microscope using the 532-nm laser as an excitation source. Total and diffuse reflectance of the films was measured over a wavelength range of 200–800 nm, using a double-beam UV-Vis-NIR spectrophotometer (Cary 5000, Varian) with an internal diffuse reflectance accessory consisting of a 110-mm-diameter integrating sphere. Baseline was recorded with a polytetrafluoroethylene (PTFE) reference disk, which exhibits NIR performance superior to traditional coatings [22] while maintaining UV-Vis performance.

3. Results

3.1. XRD results of films

The crystalline quality and orientation of the ZnO thin films on Si(100) were investigated by means of XRD. After the deposition, a PFCVAD ZnO film was annealed at 850 °C with 1 h of annealing time in air.

The crystal lattice constant c and the interplanar distance of the diffracting planes d were identified using the Bragg equation $n\lambda = 2d\sin\theta$, where n is the order of the diffracted beam, λ is the wavelength of the X-ray, and θ is the angle between the incoming X-ray and the diffracting planes. The grain sizes of the crystallites were determined from XRD data. The crystallite grain size D can be estimated using the Scherrer formula [23]:

$$D = \frac{0.9\lambda}{\beta cos\theta}, \quad (1)$$

where λ is the X-ray wavelength, θ is the Bragg diffraction angle, and β is the full width at half maximum (FWHM) in radians.

Figure 1 shows the XRD patterns of the Si substrate, the Si substrate annealed in air at 850 °C, the as-deposited ZnO, and ZnO film annealed in air at 850 °C. The bottom line belongs to the Si(100) substrate, followed by the results obtained after annealing at 850 °C with 1 h of annealing time. The third line was obtained for the as-deposited ZnO and the fourth for the ZnO film annealed at 850 °C. The values of the peak position, peak intensity, FWHM, grain size, and interplanar distance d for the ZnO thin films are reported in the Table. The peak (002) was shifted towards a higher angle by annealing at 850 °C. This angle shift was caused by a decrease in the c axis lattice constant of the ZnO thin film. This depends on relaxation of the tensile strain existing along the c-axis in the ZnO films [24–27].

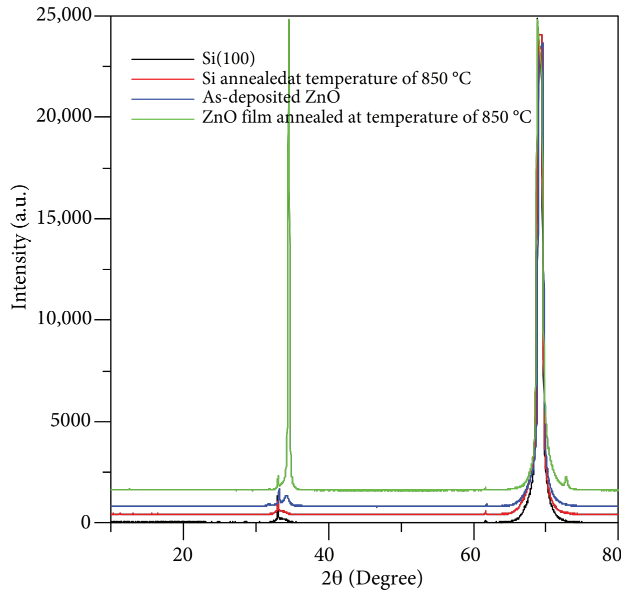

Figure 1. XRD spectra of as-deposited and annealed ZnO film.

Table. Values of the peak position, peak intensity, FWHM, grain size, and interplanar distance d for the ZnO thin films.

	Si(100)	Si annealed at 850 °C	As-deposited ZnO	ZnO film annealed at 850 °C
Angle 2θ (°)	33.0 61.7 69.1	33.0 61.7 69.1	31.7 (ZnO, (100)) 33.2 34.1 (ZnO, (002)) 61.8 69.2	31.8 (ZnO, (100)) 33.0 34.5 (ZnO, (002)) 61.7 69.1 72.7 (ZnO, (004))
Relative peak intensity	1370 163 2.89×10^5 Si(100)	7.50×10^2 178 2.87×10^5	138 (ZnO, (100)) 919 581 (ZnO, (002)) 151 272	94.0 (ZnO, (100)) 720 2.32×10^4 (ZnO, (002)) 178 2.89×10^5 693 (ZnO, (004))
FWHM (°)			1 (ZnO, (002))	0.2 (ZnO, (002))
d (nm)			0.2627 (ZnO, (002))	0.2598 (ZnO, (002))
c (nm)			0.5254 (ZnO, (002))	0.5196 (ZnO, (002))
Grain size (D), nm			8.314 (ZnO, (002))	41.61 (ZnO, (002))

It was also observed that the FWHM changed with annealing temperature. The (002) peak of the annealed ZnO film was stronger and sharper than that of the as-deposited ZnO. These results indicate that the rise of (002) peak intensity was generally related to an improvement of the crystal quality of the ZnO films and an enlargement of the grain size. As-deposited ZnO and annealed ZnO film had a weak peak (100) orientation at $2\theta = 31.7°$ and 31.8°, respectively. For ZnO film annealed at 850 °C, along with a strong (002) diffraction peak, a weak (004) diffraction peak could be found.

3.2. Raman results

Figure 2 shows the Raman scattering spectra of films excited by the 532-nm laser lines using laser power of 2 mW. A peak of 434.5 cm^{-1} is observed in as-deposited ZnO at the laser power of 2 mW [28]. This peak corresponds to the E2 (high) mode of hexagonal ZnO. However, 2 peaks are seen for ZnO film annealed in air at 850 °C with 1 h of annealing time. The Raman peaks at 100 cm^{-1} and 436.5 cm^{-1} correspond to E2 (low) mode and E2 (high) mode of hexagonal ZnO [29,30]. The FWHM of the E2 (high) peak became narrower after annealing. In wurtzite ZnO crystals, the nonpolar phonon modes with symmetry E2 have 2 frequencies; E2 (high) is associated with oxygen atoms and E2 (low) is associated with the Zn sublattice [31–33].

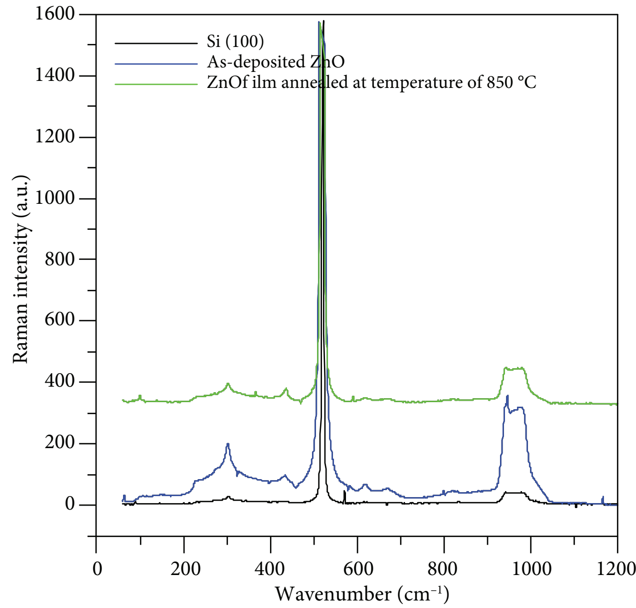

Figure 2. The Raman spectra of as-deposited and annealed ZnO thin film annealed at 850 °C.

3.3. Optical results of films on Si substrate

The optical properties of as-deposited ZnO and ZnO film annealed at 850 °C on Si substrate were studied using a Varian Cary 5000 model UV-Vis-NIR spectrophotometer with an integrating sphere, using PTFE as the reference disk. Reflectance spectra were taken in the range of 200–800 nm and in air at room temperature.

The diffuse reflectance of the sample is related to the Kubelka–Munk function F(R). The Kubelka–Munk function was used to convert reflectance measurements into equivalent absorption spectra. The Kubelka–Munk theory allows us to calculate the energy gap of the thin films on nontransparent substrates. Diffuse reflectance data were transformed using the Kubelka–Munk function by the following relation:

$$F(R) = \frac{(1-R)^2}{2R} = \frac{K}{s}, \tag{2}$$

where $R$is the diffuse reflectance of the sample; F(R) is the Kubelka–Munk function, which corresponds to the absorbance; K is the absorption coefficient; and s is the scattering coefficient. The absorption coefficient of a direct band gap semiconductor is related to Tauc's equation [34,35]:

$$\alpha h\nu = A\left(h\nu - E_g\right)^n, \tag{3}$$

where α is the linear absorption coefficient of the material, $h\nu$ is the photon energy, A is a proportionality constant, n is a constant accounting for the type of optical transition, and $n = 1/2$ indicates direct allowed transition. The Kubelka–Munk function is directly proportional to the absorbance ($\alpha = F(\mathrm{R})/t$, where t is the thickness of the film) [36].

Figure 3 shows the total reflectance spectra of the as-deposited and annealed ZnO thin films. It is observed that the total reflectance for ZnO thin film increases with annealing temperature. UV-Vis diffuse reflectance spectroscopy was used to study the optical properties of ZnO, measured at room temperature in the wavelength range of 200–800 nm. Diffuse reflectance spectra of as-deposited and annealed ZnO film are shown in Figure 4. According to the graph of $F(\mathrm{R})$ versus energy values (Figure 5), the UV-absorption band of the as-deposited and annealed ZnO film was around 360–390 nm. The energy band gap of films was calculated by plotting the square of the Kubelka–Munk function versus energy (Figure 6). Extrapolating the linear portion of the curve onto the x-axis gives the energy band gap of the films. The estimated band gap energy values are 3.00 and 3.28 eV for films as-deposited and annealed at 850 °C, respectively. The increase in the band gap may be due to the improved crystalline structure of the ZnO thin films with the increase in annealing temperature. It has been proposed that most annealing treatments cause evaporation of oxygen and the samples thus become more Zn-rich. As O-rich samples usually have lower band gap energies, relatively more Zn-rich samples after annealing, due to the evaporation of excess oxygen from the surface, will have higher band gap energies in comparison to the as-deposited samples [37].

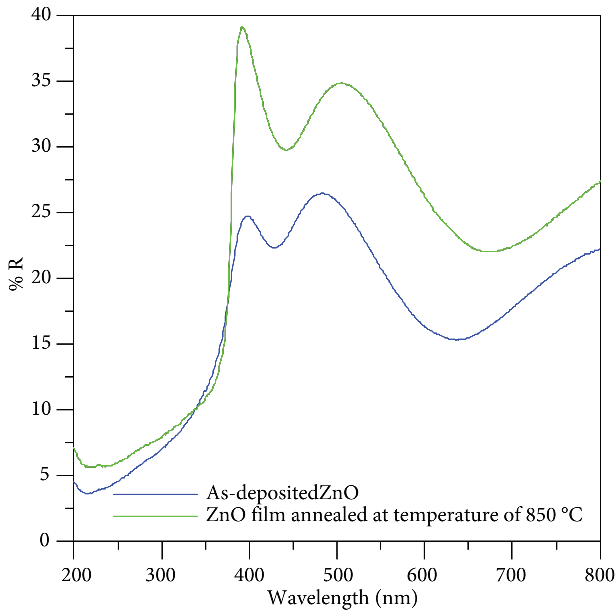

Figure 3. Total reflectance spectra of ZnO film as-deposited and annealed.

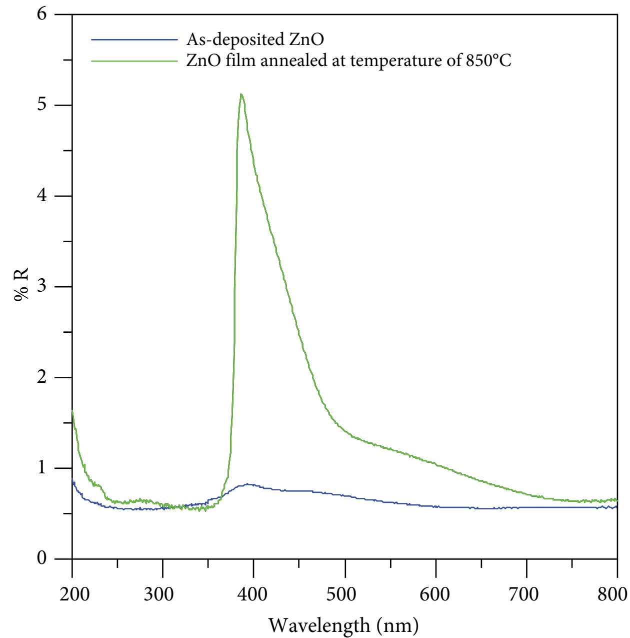

Figure 4. Diffuse reflectance spectra of films.

4. Conclusion

The crystallinity and optical properties of ZnO/p-Si were investigated. The conclusion of this study is that all the films exhibited preferential (002) orientation with c-axis perpendicular to the substrate surface, which indicated that the ZnO thin films were of hexagonal wurtzite crystal structure. Additionally, the (004) peak

was seen for film annealed at 850 °C. The band gap energy estimated for films as-deposited and annealed at 850 °C was 3.00 and 3.28 eV, respectively. One Raman peak was observed for as-deposited ZnO at the laser power of 2 mW. However, 2 Raman peaks were observed for ZnO film annealed in air at 850 °C with 1 h of annealing time. Those peaks correspond to modes of hexagonal ZnO. These results suggest that PFCVAD may be a good candidate to produce ZnO/p-Si heterojunctions for device applications such as ZnO-based devices.

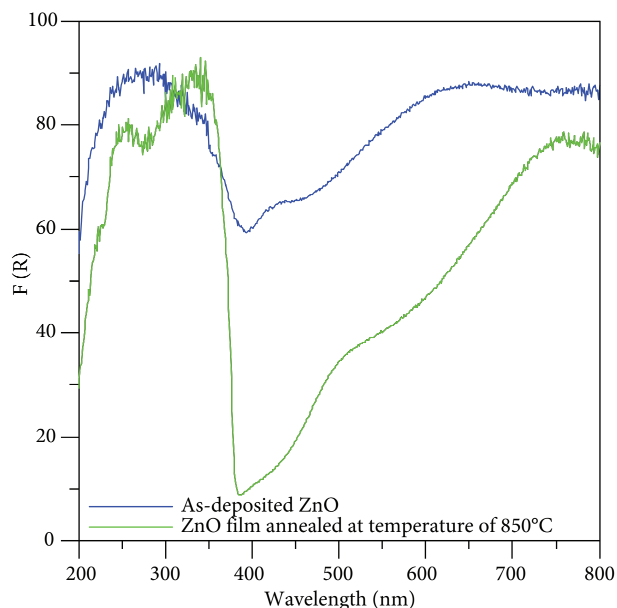

Figure 5. $F(R)$ against wavelength for ZnO film as-deposited and annealed for 1 h.

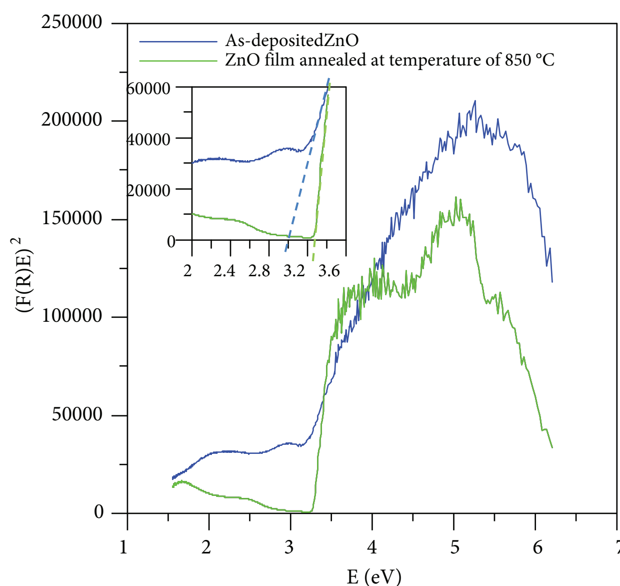

Figure 6. $(F(R)\mathrm{E})^2$ against energy of films.

Acknowledgment

The authors thank Özge Bağlayan from Anadolu University for Raman measurements.

References

[1] Kim, H. W.; Kebede, M. A.; Kim, H. S. *Curr. Appl. Phys.* **2010**, *10*, 60–63.

[2] Yamada, H.; Ushimi, Y.; Takeuchi, M.; Yoshino, Y.; Makino, T.; Arai, S. *Vacuum* **2004**, *74*, 689–692.

[3] Tominaga, K.; Murayama, T.; Mori, I.; Okamoto, T.; Hiruta, K.; Moriga, T.; Nakabayashi, I. *Vacuum* **2000**, *59*, 546–552.

[4] Qi, H.; Li, Q.; Wang, C.; Zhang, L.; Lv, L. *Vacuum* **2007**, *81*, 943–946.

[5] Xiao, Z. Y.; Liu, Y. C.; Zhao, D. X.; Zhang, J. Y.; Lu, Y. M.; Shen, D. Z.; Fan, X. W. *J. Lumin.* **2007**, *122–123*, 822–824.

[6] Xu, Q.; Cheng, Q.; Zhang, Z.; Hong, R.; Chen, X.; Wua, Z.; Zhang, F. *J. Alloy. Compd.* **2014**, *590*, 260–265.

[7] Cheng, Q.; Ostrikov, K. *Cryst. Eng. Comm.* **2011**, *13*, 3455–3461.

[8] Cheng, Q.; Ostrikov, K. *Chem. Phys. Chem.* **2010**, *13*, 1535–1541.

[9] Sun, K.; Jing, Y.; Li, C.; Zhang, X.; Aguinaldo, R.; Kargar, A.; Madsen, K.; Banu, K.; Zhou, Y.; Bando, Y.; et al. *Nanoscale* **2012**, *4*, 1515–1521.

[10] Wei, M.; Boutwell, R. C.; Garrett, G. A.; Goodman, K.; Rotella, P.; Wraback, M.; Schoenfeld, W. V. *J. Alloy. Compd.* **2013**, *552*, 127–130.

[11] Lee, J. Y.; Choi, Y. S.; Choi, W. H.; Yeom, H. W.; Yoon, Y. K.; Kim, J. H.; Im, S. *Thin Solid Films* **2002**, *420–421*, 112–116.

[12] Khranovskyy, V.; Ulyashin, A.; Lashkarev, G.; Svensson, B. G.; Yakimova, R. *Thin Solid Films* **2008**, *516*, 1396–1400.

[13] Fang, Z.; Wang, Y.; Xu, D.; Tan, Y.; Liu, X. *Opt. Mater.* **2004**, *26*, 239–242.

[14] Mansour, S. A.; Yakuphanoglu, F. *Solid State Sci.* **2012**, *14*, 121–126.

[15] Heitsch, S.; Bundesmann, C.; Wagner, G.; Zimmermann, G.; Rahm, A.; Hochmuth, H.; Benndorf, G.; Schmidt, H.; Schubert, M.; Lorenz, M.; et al. *Thin Solid Films* **2006**, *496*, 234–239.

[16] Guo, B.; Ye, Z.; Wong, K. S. *J. Cryst. Growth* **2003**, *253*, 252–257.

[17] Shimizu, M.; Shiosaki, T.; Kawabata, A. *J. Cryst. Growth* **1982**, *57*, 94–100.

[18] Jian, S. R.; Lee, Y. H. *J. Alloy. Compd.* **2014**, *587*, 313–317.

[19] Cho, S. G.; Lee, D. U.; Pak, S. W.; Nahm, T. U.; Kim, E. K. *Thin Solid Films* **2012**, *520*, 5997–6000.

[20] Xu, X.; Guo, C.; Qi, Z.; Liu, H.; Xu, J.; Shi, C.; Chong, C.; Huang, W.; Zhou, Y.; Xu, C. *Chem. Phys. Lett.* **2002**, *364*, 57–63.

[21] Şenadım, E.; Kavak, H.; Esen, R. *J. Phys.-Condens. Mat.* **2006**, *186*, 6391–6400.

[22] Weidner, V. R.; Hsia, J. J. *J. Opt. Soc. Am.* **1981**, *71*, 856–861.

[23] Hashim, A. J.; Jaafar, M. S.; Ghazai, A. J.; Ahmed, N. M. *Optik* **2013**, *124*, 491–492.

[24] Yuk, J. M.; Shin, J. W.; Lee, J. Y. *J. Korean Phys. Soc.* **2007**, *50*, 608–611.

[25] Fang, Z. B.; Yan, Z. J.; Tan, Y. S.; Liu, X. Q.; Wang, Y. Y. *Appl. Surf. Sci.* **2005**, *241*, 303–308.

[26] Gupta, V.; Mansingh, A. *J. Appl. Phys.* **1996**, *80*, 1063–1073.

[27] Zhang, Y.; Du, G.; Liu, D.; Wang, X.; Ma, Y.; Wang, J.; Yin, J.; Yang, X.; Hou, X; Yang, S. *J. Cryst. Growth* **2002**, *243*, 439–443.

[28] Zhang, Y.; Du, G.; Yang, X.; Zhao, B.; Ma, Y.; Yang, T.; Ong, H. C.; Liu, D.; Yang, *S. Semicond. Sci. Technol.* **2004**, *19*, 755–758.

[29] Li, C. P.; Yang, B. H.; Wang, X. C.; Wang, F.; Li, M. J.; Su, L.; Li, X. W. *Appl. Surf. Sci.* **2011**, *257*, 5998–6003.

[30] Hammouda, A.; Canizarès, A.; Simon, P.; Boughalout, A.; Kechouane, M. *Vib. Spectrosc.* **2012**, *62*, 217–221.

[31] Calizo, I.; Alim, K. A.; Fonoberov, V. A.; Krishnakumar, S.; Shamsa, M.; Balandin, A. A.; Kurtz, R. *Proc. of SPIE* **2007**, *6481*, 64810N-1.

[32] Alim, K.; Fonoberov, V. A.; Shamsa, M.; Balandin, A. A. *J. Appl. Phys.* **2005**, *97*, 124313-1-5.

[33] Ashkenov, N.; Mbenkum, B. N.; Bundesmann, C.; Riede, V.; Lorenz, M.; Spemann, D.; Kaidashev, E. M; Kasic, A.; Schubert, M.; Grundmann, M.; et al. *J. Appl. Phys.* **2003**, *93*, 126–133.

[34] Tauc, J.; Menth, A. *J. Non-Cryst. Solids* **1972**, *8–10*, 569–585.

[35] Kako, T.; Kikugawa, N.; Ye, J. *Catal. Today* **2008**, *131*, 197–202.

[36] Yakuphanoglu, F. *J. Alloy. Compd.* **2010**, *507*, 184–189.

[37] Coşkun, C.; Güney, H.; Gür, E.; Tüzemen, S. *Turk. J. Phys.* **2009**, *33*, 49–56.